IEEE Access
Multidisciplinary | Rapid Review | Open Access Journal

Received May 31, 2019, accepted July 1, 2019, date of publication July 8, 2019, date of current version July 31, 2019.

Digital Object Identifier 10.1109/ACCESS.2019.2927377

Simulation and Validation of the Air Flow generated by a Multi-Channel Air-Assisted Sprayer

XIANGYUN CHAO[1], SHANG CHEN[1], WEI QIU[1], XIAOLAN LV[2], HUA LI[1], CHANGJIE HAN[3], AND FIAZ AHMAD[4,5]

[1]Nanjing Agricultural University, Nanjing 210000, China
[2]Jiangsu Academy of Agricultural Sciences, Nanjing 210000, China
[3]Xinjiang Agricultural University, Ürümqi 830001, China
[4]School of Equipment Engineering, Jiangsu University, Zhenjiang 212013, China
[5]Department of Agricultural Engineering, Bahauddin Zakariya University, Multan 60000, Pakistan

Corresponding author: Wei Qiu (qiuwei@njau.edu.cn)

This work was supported in part by the National Natural Science Foundation of China under Grant 51805271, in part by the Fundamental Research Funds for the Central Universities under Grant KYYJ201805, in part by the Jiangsu Agricultural Science and Technology Innovation Fund under Grant CX181007, and in part by the Nanjing Agricultural University SRT under Grant 20181037084.

ABSTRACT The multi-channel air-assisted spraying can distribute air flow according to the crown diameter and be helpful to improve spray deposition and in the reduction of environmental pollution. However, the factors of air flow distribution are not clear. Computational fluid dynamics (CFD) simulation was used in this paper to investigate the influence of the fan speed (600–1800 rpm) and the distance from the air outlet (0–6.0 m) on the airflow field distribution. The measurements and the simulation results were consistent within the boundary of the test range. The results indicated that the airflow field in the central plane was basically axis-symmetric. The airflow field diffused in the central plane at a certain angle of diffusion. The air velocity first increased and then gradually decreased along the central line, and it displayed an exponential function. Within the range of 1.0 m from the air outlet, there was an obvious section of static air between the adjacent air outlets. Beyond this range, the airflow was well-distributed, and the air velocity was normally distributed at the height y. The airfield generated by the multi-channel sprayer was elliptical in its cross-section from the outlet (for $x > 1.0$ m). The distance of the air supply significantly influenced the fluctuation of the velocity of the airflow, while the speed of the fan had no significant influence on the position of the confluence point of the airflow and the fluctuation of the velocity of each test section.

INDEX TERMS Chemical industry, computational fluid dynamics, open area test sites, waste reduction, multi-channel sprayer.

I. INTRODUCTION

Pesticides spray plays a significantly important role in providing high-quality crops and enhancing the productivity. However, excessive use of pesticides can pose serious environmental and health hazards. Air-assisted variable spray technology can significantly reduce pesticide usage in orchards [1]–[4]. Airflow is a key parameter that determines the effect of the application of air-assisted variable spray technology and influences the control efficacy. However, the operators often adjust the unit's flow parameters using their experience due to the lack of an air flow distribution law. Unreasonable air outlet speeds and positions can cause drift and non-internal deposition.

Accurate description of the flow field characteristics and influencing factors for orchard sprayers is a challenging and hot topic. Scholars have taken initiatives to change the air volumetric flow rate [5], [6], the air outlet speed [7], [8], and the air outlet height [9] according to the canopy characteristics [6], [10], [11]. Increasing the number of fans [12], adding an air flow conversion device [13], adjusting the outlet shape [14], setting the deflector [15], using a windshield

The associate editor coordinating the review of this manuscript and approving it for publication was Qiang Lai.

plate to adjust the air volume [16]–[18], and using hydraulic stepless speed regulation [19] to change the speed of the fan are considered to be the effective ways to change the air flow field.

However, the crowns of fruit trees are irregular, in other words, volume and biomass for different crown diameters are also different; therefore, the amount of air and pesticides required for crowns with different diameters are also different. The above-mentioned study reflects that the airflow regulations between canopies were emphasized upon; nonetheless, little attention has been paid to a single canopy. Multi-channel air-assisted spray technology was utilized by some scholars, as it realizes independent adjustment of the airflow parameters of various channels [20]. Thus, the air velocity [21] and drift [22] of the vertical spray profiles can be observed and adjusted to meet the demands of crown with different diameters.

The multi-channel sprayer essentially consists of multiple air outlets that produce several jets. However, it is not the superposition of a single air jet. Although some researches have been carried out related to the jet characteristics of a single fan or an air outlet [23]–[26], relatively little is known about the airflow generated by multi channels, and even less is known about the law of velocity change after the coincidence of the airflow. At present, description of the distribution law of airflow field of multi-channel sprayer is still a challenging task. The airflow field regulation strategies of the multi-channel sprayer are beneficial. Based on these strategies, the air flow for different canopy regions can be adjusted accurately, not relying on experience.

Therefore, spatial distribution of air and variation rules of the multi-channel air-assisted sprayer were investigated in detail in this study. The primary objectives were as follows: (1) investigation of the effects of the fan speed and distance on the distribution of the airflow field; (2) obtaining a calculation method for the airflow field of the multi-channel sprayer, providing a fundamental basis for accurate adjustment of the airflow based on a single canopy.

II. MATERIALS AND METHODS

A. AIR SPRAYER

An air-assisted sprayer with multiple channels was used in this study, which mainly consisted of a spray system, an air-assisted system, and a power system (Fig. 1). A mixed, uneven flow field was generated using four symmetrical channels on each side. The axial-flow fan was driven by a electromotor (power: 11kw, when n = 1450r m^{-1}), and can be stepless speed regulation (0-2000r min^{-1}). A curved dome was installed in outlet of the fan. Eight short arms (diameter: 100mm) were arranged along circumference in the curved dome and connected to air outlets (diameter:110 mm) with hoses. Air outlets were arranged symmetrically on both sides, spaced at 300 mm intervals. The height adjustment range of air outlet was between 800 and 2000 mm, in order to adapt to the low dense orchard. Each outlet has a wind valve, which

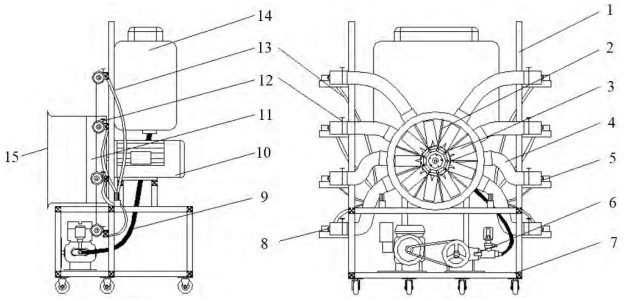

FIGURE 1. Schematic illustration of a multi-channel sprayer (Note: 1 Frame, 2 Diffuser, 3 Fan, 4 Air Duct, 5 Spray Nozzle, 6 Pesticide Pump, 7 Mobile Station, 8 Outlet of Sprayer, 9 Hose, 10 Power Source, 11 Rear Arc Cover, 12 Air Valve, 13 Tube, 14 Pesticide Tank, 15 Air Inlet.).

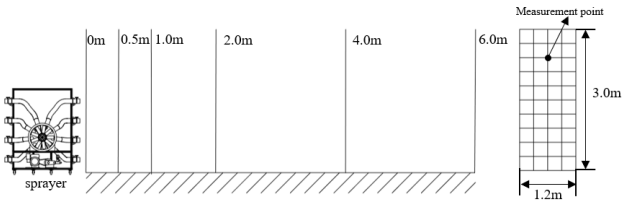

FIGURE 2. Distribution of the measurement points.

is used to adjust the airflow speed (range: 0-40 m s^{-1}), and the nozzle (type: cone nozzle; flowrate:1.2 L min^{-1}) is placed outside the outlet.

B. EXPERIMENTAL MEASUREMENTS

The airflow distribution characteristics of the multi-channel sprayer were measured using the TSI 9565 hot wire anemometer (TSI Inc., Minnesota, USA) at six different fan speeds (600, 900, 1200, 1500, and 1800 r min^{-1}). The layout of the measurement points is shown in Fig. 2. The total test length was 6.0 m, with measurement points at 0, 0.5, 1.0, 2.0, 4.0, and 6.0 m on the cross section of the test points. The height of the test interval was 0.3 m (starting from 0.1 m above the ground), and the width was 0.3 m. Each data point was measured three times; and the mean value was taken as the wind speed of the measurement points, the on-site testing is shown in Fig. 3.

C. FORMULATION OF THE MODEL

A CFD model was developed using the CFD package FLUENT (ANSYS, Inc., Canonsburg, Pennsylvania, USA). The simulation of the airflow was mainly based on the conservation of mass equation and conservation of momentum in the Navier–Stokes (N–S) equations was the basis of the airflow simulation for the multichannel sprayer.

1) GOVERNING EQUATIONS

The flow field was iterated using the k-e turbulence model, the material transport mode, and the standard wall function. The general control formulas are as follows [27]:

$$\frac{\partial(\rho\phi)}{\partial t} + \mathrm{div}(\rho u \Phi) = \mathrm{div}(\Gamma\, \mathrm{grad}\, \Phi) + S \qquad (1)$$

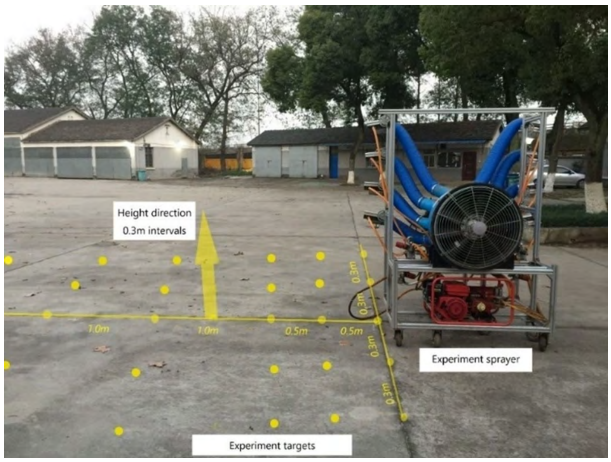

(a) Setting of measurement point

(b) Test equipment

FIGURE 3. The on-site testing.

For which the expansion form is:

$$\frac{\partial(\rho\phi)}{\partial t}+\frac{\partial(\rho u\phi)}{\partial x}+\frac{\partial(\rho u\phi)}{\partial y}+\frac{\partial(\rho u\phi)}{\partial z}=\frac{\partial}{\partial x}\left(\Gamma\frac{\partial\phi}{\partial x}\right)+\frac{\partial}{\partial y}\left(\Gamma\frac{\partial\phi}{\partial y}\right)+\frac{\partial}{\partial z}\left(\Gamma\frac{\partial\phi}{\partial z}\right)+S \quad (2)$$

where

$\boldsymbol{\rho}$ = the model's density (kg m^{-3})

$\boldsymbol{\Phi}$ = the universal variable, representing dependent variables u, v, and w etc., where u, v, and w are components of the velocity vector on the X, Y, and Z axes, respectively

t = time (s)

u = the velocity vector (m s^{-1})

T = the temperature (°C)

Γ = the generalized diffusion coefficient

S = the generalized source item.

Related manual should be consulted for other parameters.

2) GEOMETRY AND THE BOUNDARY CONDITIONS

Including the entire experimental hall volume, the machine and the geometry of the tractor in the simulation was computationally demanding. Therefore, a simplified free space domain with dimensions of 6.0 m × 3.0 m × 2.4 m was used (Fig. 4). The four vents of the sprayer were defined as the inlets of the outflow field. Due to the different lengths of the air ducts, the air velocities from the outlets 1-4 differ from each other. The wind speed was set according to the preliminary experiment (Table 1).

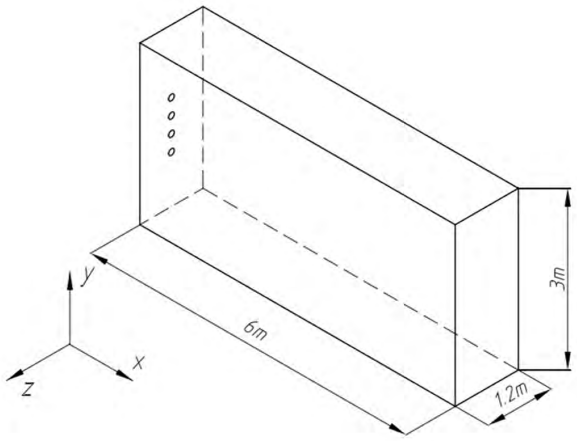

FIGURE 4. Geometry of the CFD model.

TABLE 1. Settings of the entry boundary conditions.

Fan speed (r·min^{-1})	Air velocity (m·s^{-1})			
	Outlet 1	Outlet 2	Outlet 3	Outlet 4
600	7.29	8.69	9.07	8.92
900	11.76	13.56	16.00	14.34
1200	14.59	17.85	21.08	19.37
1500	18.24	23.15	25.81	22.02
1800	23.15	26.88	29.78	27.48

3) CONTROL VOLUME MESH AND THE SOLUTION PROCEDURE

ICEM CFD was used for generating the mesh model; the grid was divided into a tetrahedral and an unstructured grid with strong applicability, and the entry and exit grids were encrypted. At each time step for the transient simulation and after 498 iterations in a stable environment, the solution converged to a normalized root mean square (RMS) residual of a value below 10^{-6} of all the equations.

III. RESULTS AND DISCUSSION

A. THE SHAPE OF THE AIR JET

The CFD simulation results showed the air velocity in a convex pattern for fan speeds of 600, 900, 1200, 1500, and 1800 r min^{-1}, respectively. Fig. 5 expressed central plane and the cross-section velocity field profile at 0, 0.5, 1.0 2.0, and 4.0 m away from the outlets at 1500 r min^{-1}. The results related to velocity distribution characteristics of the air flow field were accordingly to previous studies [28], [29]. At a certain fan speed, the loss head alone in the pipeline is directly proportional to the length of the air duct. The air velocity of the outlets decreases with the increase in the length of the air duct [30].

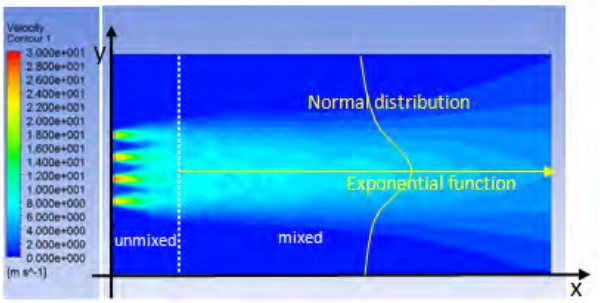

(a) Central plane

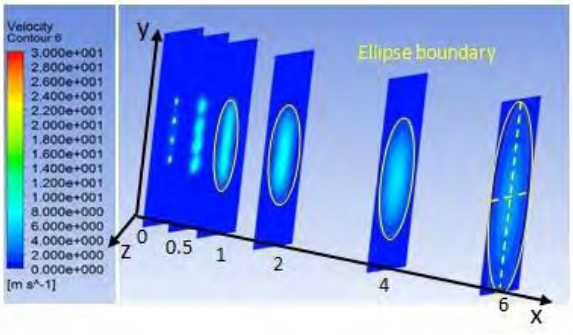

(b) Different distance sections from the outlet

FIGURE 5. Airflow field cloud map at a fan speed of 1500 r min^{-1}.

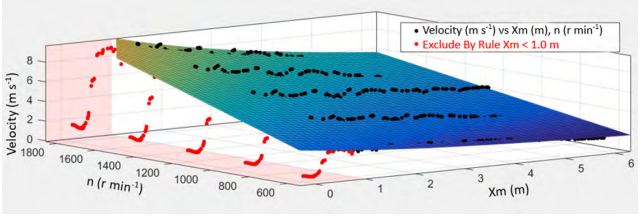

FIGURE 6. Air velocity at the center line for different fan speeds.

Fig. 5(a) demonstrates that the airflow velocity field basically displays an axisymmetric shape in the central plane. Within the range of 1.0 m from the outlet, the distribution of the air flow field was not uniform, and there were obvious areas of static air between the adjacent outlets. The velocity of the air gradually increased along the central line. When the distance from the outlet was greater than 1.0 m, the air flow was uniformly mixed and diffused in the central plane at a certain angle of diffusion.

MATLAB was then used to simulate the air velocity at the central line for different fan speeds (Fig. 6). The results indicated that the air velocity u_m on the central line basically satisfied the following equation:

$$u_m = \frac{0.001 \times \mathrm{n}}{0.027\,x + 0.162}, \quad \mathrm{x} \geq 1 \tag{3}$$

where

u_m = the air velocity at the center line (m s^{-1})
n = the fan speed (r min^{-1})
x = the distance from the air outlets (m).

The velocity distribution at the height y in the region where there was uniform mixing of the air (i.e. within a distance of more than 1.0 m from the air outlet) was basically Gaussian, which can be expressed by using the following semi-empirical formula [31], [32]:

$$\frac{u}{u_m} = \exp\left(-\frac{y^2}{a^2}\right), \quad \mathrm{x} \geq 1 \tag{4}$$

where

u_m = the velocity of the air on the central axis (m s^{-1})
u = the air velocity at different heights at the same distance from the air supply (m s^{-1})
y = the distance from the central line (m)
a = half of the thickness of the boundary of the air flow field (m).

By substituting Formula (3) into Formula (4), the velocity of the air flow at each point in the region of uniform air flow in the central plane (i.e. beyond the range of 1.0 m from the outlets) can be obtained, as shown in the following equation:

$$\mathrm{u} = \frac{0.001 \times \mathrm{n}}{0.027\,x + 0.162} \exp\left(-\frac{y^2}{a^2}\right), \quad \mathrm{x} \geq 1 \tag{5}$$

where

u = the velocity of the air in the central plane (m s^{-1})
n = the fan speed (r min^{-1})
x = the distance from the air supply (m)
y = the distance from the central line (m)
a = half of the thickness of the boundary of the air flow field (m).

Fig. 5(b) clearly represents that the four strands of airflow that were produced by the multi-channel sprayers begin to intersect at a distance of 0.5 m from the outlet. They are almost completely mixed before the 1.0 m line, and the mixed airflow field radiates out along the central line in an approximately oval shape. With the increase in the distance from the outlets, the distribution range of the airflow field becomes larger; changing from a multi-level small elliptical distribution to a small-level large elliptical distribution.

In order to clearly express the distribution in each section beyond the outlet (x $\geq$ 1.0m), the ellipse can be described as follows:

$$\frac{\mathrm{x}^2}{\mathrm{a}^2} + \frac{\mathrm{y}^2}{\mathrm{b}^2} = 1 \tag{6}$$

where

a = the length of the semi-major axis
b = the length of the semi-minor axis.

The line formed by the center (X, Y) of the ellipse in each section was perpendicular to each section, and its coordinates were independent of the distance from the air supply. The semi-major axis 'a' and the semi-minor axis 'b' increased linearly with the increase of the distance from the air supply; the relationship for this is represented as follows:

$$\mathrm{a} = 0.527 \times e^{0.1344\,x}, \quad \mathrm{x} \geq 1 \tag{7}$$

$$\mathrm{b} = 0.505\mathrm{x} + 0.067, \quad \mathrm{x} \geq 1 \tag{8}$$

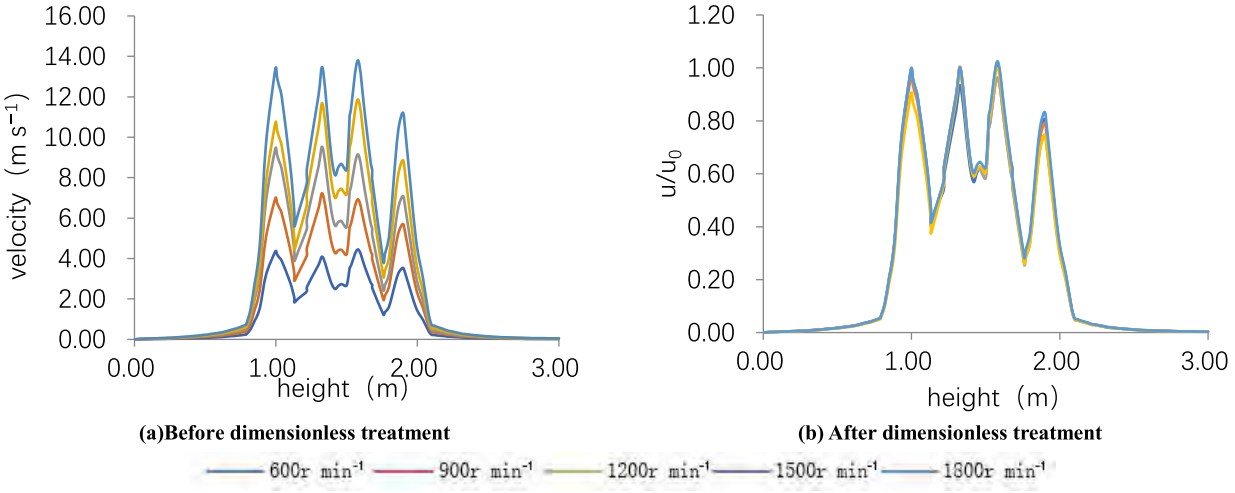

FIGURE 7. Velocity curves of the different fan speeds for the section 0.5 m from the outlets.

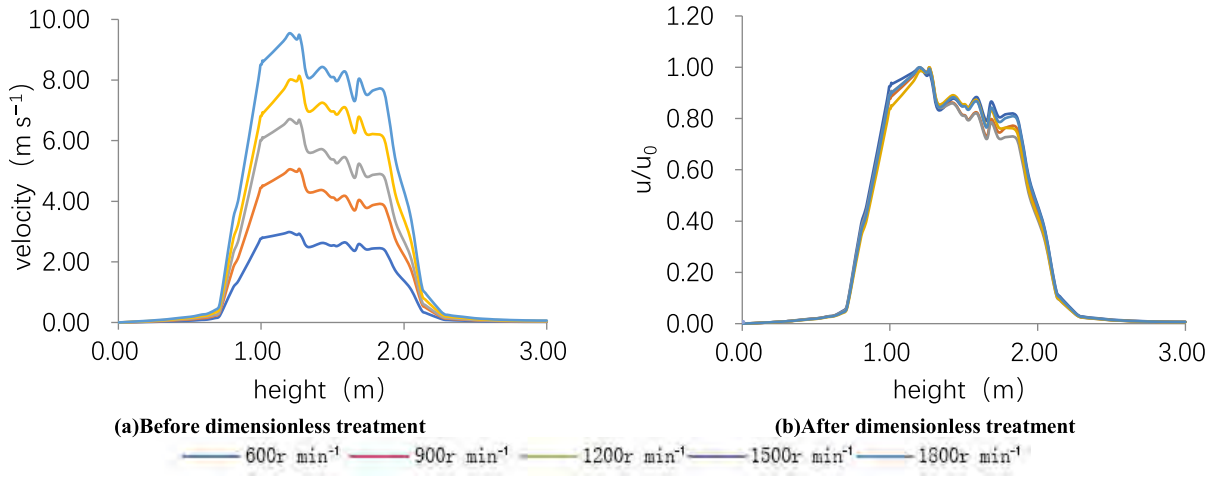

FIGURE 8. Velocity curves of the different fan speeds for the section 1.0 m from the outlets.

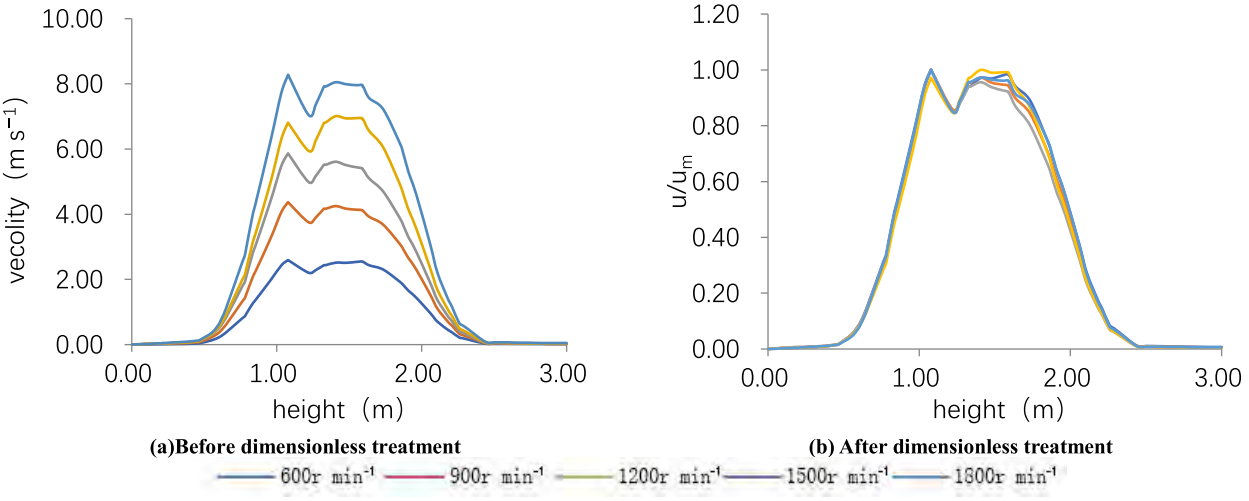

FIGURE 9. Velocity curves of the different fan speeds for the section 2.0 m from the outlets.

If the distance from the outlet is known (when x is greater than 1.0 m), the length of the semi-major axis and the semi-minor axis of the section can be obtained, and then the ellipse distribution rule of the section can be found.

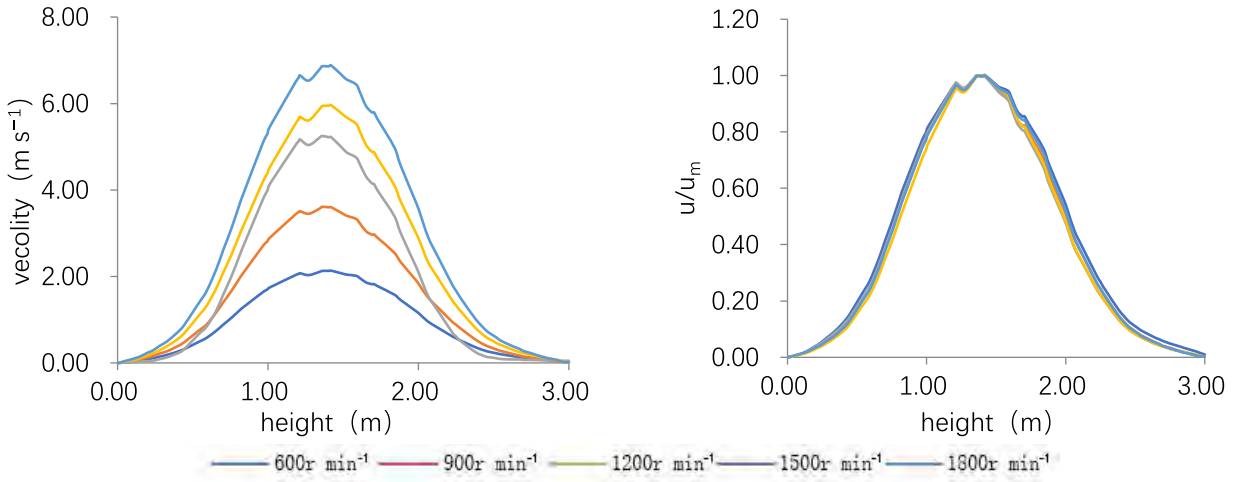

FIGURE 10. Velocity curves of the different fan speeds for the section 4.0 m from the outlets.

TABLE 2. Location of the air flow confluence point at the different fan speeds.

Fan speed (r min^{-1})	The distance between the different air confluence points and the outlets(m)			
	Air confluence points of outlets 1、2	Air confluence points of outlets 2、3	Air confluence points of outlets 3、4	Air confluence points of all the outlets
0	0.97	1.02	0.97	1.02
900	0.95	0.99	0.95	0.99
1200	0.95	0.98	0.95	0.98
1500	0.94	0.98	0.94	0.98
1800	0.94	0.99	0.94	0.99

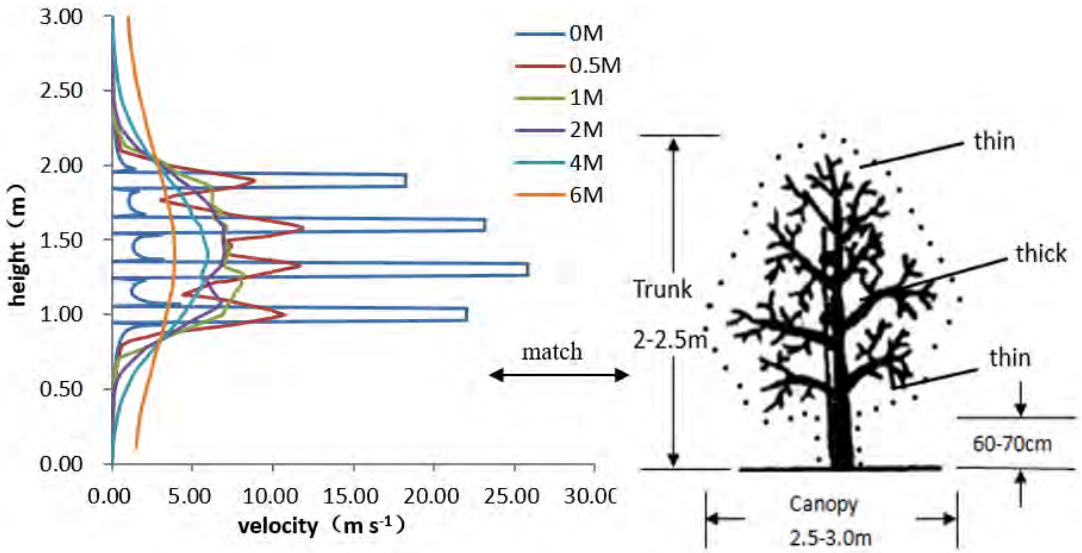

(a)Airflow velocity for the different distances from the air supply (b) Spindle tree

FIGURE 11. Profiling modeling spray.

B. EFFECT OF THE FAN SPEED ON THE AIRFLOW FIELD

The effect of the fan speeds (600, 900, 1200, 1500, and 1800 r min^{-1}) on the air flow velocity distribution at 0.5, 1.0, 2.0, and 4.0 m from the outlet are shown in the Figs. 7–10.

From the simulation results it was clearly observed that outlet velocity increased with the increase in the fan speed and the airflow velocity after the mixing of the flows also increased. After the data were transformed by dimensionless theory [33], the variation trends of the curves were found to be similar under the different fan speeds. When the distance between the vents was constant, the fluctuation of the air flow did not change. Whereas, the fan speed changed at a distance

TABLE 3. Comparison of the simulation and the test values.

Height(m)	Airflow velocity test, simulation and relative error								
	Group A (0 m)			Group B (0.5 m)			Group C (1.0 m)		
	Measured	Simulated	E/%	Measured	Simulated	E/%	Measured	Simulated	E/%
0.1	0.45	0.05	-	0.30	0.03	-	0.23	0.02	-
0.4	0.51	0.10	-	0.29	0.12	-	0.20	0.13	-
0.7	0.37	0.30	19.91	0.42	0.43	2.38	0.66	0.42	36.36
1.0	21.15	22.02	4.11	10.18	10.77	5.80	5.68	6.81	19.90
1.3	23.29	25.81	10.82	11.07	10.42	5.87	5.91	7.87	33.16
1.6	22.02	23.15	5.13	11.54	11.87	2.86	5.95	7.09	19.16
1.9	17.58	18.24	3.75	8.28	8.85	6.88	4.67	5.36	14.78
2.2	0.12	0.26	-	0.47	0.41	12.76	0.54	0.67	24.07
2.5	0.12	0.09	-	0.15	0.13	-	0.23	0.10	-
2.8	0.26	0.03	-	0.13	0.05	-	0.12	0.06	-
3.1	0.14	0.01	-	0.10	0.04	-	0.15	0.05	-
Height(m)	Airflow velocity measurement, simulation and relative error								
	Group E (2.0 m)			Group F (4.0 m)			Group G (6.0 m)		
	Measured	Simulated	E/%	Measured	Simulated	E/%	Measured	Simulated	E/%
0.1	0.33	0.02	-	0.66	0.07	-	0.88	1.46	65.9
0.4	0.23	0.07	-	0.68	0.56	17.65	1.02	1.84	80.39
0.7	1.02	0.42	-	2.34	2.09	10.68	2.16	2.62	21.29
1	5.43	6.82	25.60	3.46	4.42	27.74	2.18	3.40	55.96
1.3	5.40	6.80	25.93	4.30	5.61	30.47	2.63	3.85	46.39
1.6	5.11	6.89	14.51	4.29	5.40	25.87	2.58	3.79	46.90
1.9	3.80	4.17	9.74	3.12	3.73	19.55	2.35	3.13	33.19
2.2	0.69	0.96	39.13	1.23	1.43	16.26	2.12	2.23	5.18
2.5	0.28	0.06	-	0.43	0.46	6.98	1.18	1.62	37.29
2.8	0.13	0.04	-	0.15	0.13	-	0.43	1.15	-
3.1	0.12	0.04	-	0.12	0.02	-	0.31	0.97	-

less than 0.5 m, the entrainment of the jets to the surrounding stationary fluid created a low-pressure zone between each jet stream, which resulted to two jets intersecting each other. There were four peaks in the air velocity curves, which appeared on the axis of the outlet. In the section at a distance of 0.5 m to 1.0 m, the air flow mixed violently, and there was an obvious fluctuation in the air flow and thus no obvious peak was observed. At the distance of 2.0 m, the airflows merged into a single peak. When the distance between the outlets was constant, the position of the confluence point of the air did not change when the fan speed changed: the air confluence point was about 1.0 m away from the outlet, as presented in Table 2.

C. EFFECT OF THE DISTANCE FROM THE AIR SUPPLY ON THE AIRFLOW FIELD

In order to analyze the impact of the distance from the outlets, the velocity distribution results of seven sections at a distance of 0, 0.5, 1.0, 2.0, 4.0, and 6.0 m were obtained under the condition of a fan speed of 1500 r min^{-1} (Fig. 11 (a)). At the center of the central axis (i.e., 1.45 m) the airflow velocity reached its maximum and gradually decreased as it moved to the upper and lower sides. With the increase of the distance of the airflow from the jets, the maximum airflow velocity decreased and the range of the airflow field increased. In the area less than 1 m from the outlet, the airflow distribution was not consistent with the above-mentioned results due to the incomplete cross-mixing of the four airflows. Moreover, there was a certain area where the multi-stream spray did not mix, thus the distance between the airflow outlet and the canopy should be considered.

The above-mentioned results concluded that the maximum air velocity of the sprayer at 1 m was 8 m s^{-1} when the fan speed was 1500 r min^{-1}, and the coverage height was in the range of 0.7–2.1 m. The air velocity in the middle section was large, and the upper and lower airflow forces were weak, and it matched with the thick middle crown layer and the thin upper crown layer of the spindle tree (Fig. 11 (b)). The multi-channel sprayer has been proven to have a strong profiling ability, in particular, after adjusting the angle of the nozzles.

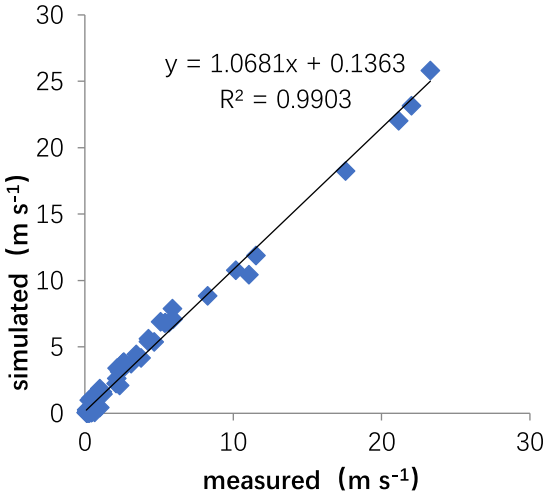

FIGURE 12. Linear correlation between the simulated and measured values.

Similarly, Reference [34] fond that the CFD model predicted that drift reducing nozzles reduced the drifting distance by 50%, but increased near-tree ground deposition.

D. COMPARISON OF THE SIMULATION RESULTS WITH THE EXPERIMENTAL RESULTS

The average relative error E was calculated by using the following equation:

$$E = \frac{|v_m - v_s|}{v_m} \times 100\% \quad (9)$$

where

E = the average relative error

v_m = the measured velocity (m s^{-1})

v_s = the simulated velocity (m s^{-1}).

The accuracy of the simulation results was similar for the different fan speeds. Table 3 summarizes the comparison between the measured results and the simulation results when the fan speed was 1500 r min^{-1}. The boundary of the airflow field was set at the point where the wind speed was below 0.3 m s^{-1}, which was not recorded.

Data listed in Table 3 indicate that the simulated results in this condition were basically consistent with the experimental results. Of the 60 points, 27 points were located outside the boundary of the airflow field. The relative error caused by the minimal wind speed was not considered. Considering the relative error for the 33 points, the relative error of the results of the 24-point simulation was less than 30%, accounting for 72.7%.

The results revealed a linear correlation between the simulated values and the test values (Fig. 12). The linear correlation equation of $y = 1.068x + 0.136$ was obtained for the data, and its determination coefficient was $R^2 = 0.990$.

According to the results of the on-site testing, the reason for the errors was that the position of the researcher disturbed the airflow field during the actual measurement. Anemometer also produced some measurement errors. At the same time, the simulation process used horizontal airflow to replace the unstable spiral airflow caused by the fan, which could also result in certain errors. The pervious related studies showed that that there are errors inherent to the implementation of the CFD model, errors related to inaccuracies in the geometry

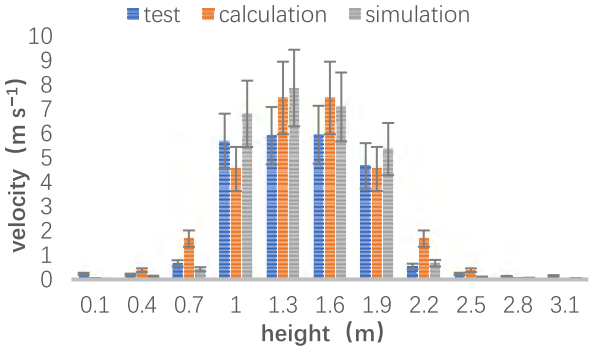

(a) Comparison of the air velocity values for the section 1.0 m from the outlets

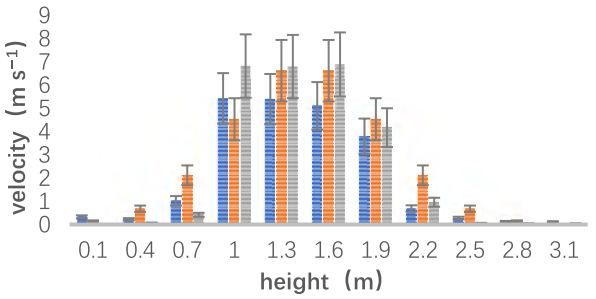

(b) Comparison of the air velocity values for the section 2.0 m from the outlets

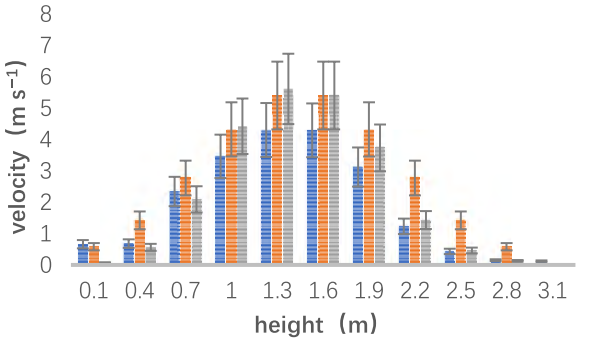

(c) Comparison of the air velocity values for the section 4.0 m from the outlets

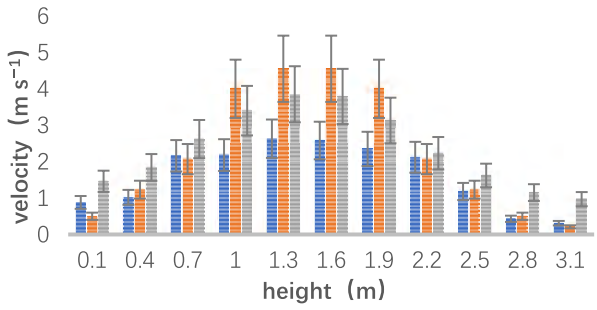

(d) Comparison of the air velocity values for the section 6.0 m from the outlets

FIGURE 13. Comparison of the calculation, simulation and test values for the different distances from the air supply.

of the air ducts, inaccuracies related to the measurement of the air velocities, inaccuracies in the quantification of the air flow, and simplifications linked to the turbulent model [35]. Reference [4] found the average RMS errors of peak air velocities and airflow pressures were 1.68ms^{-1} and 0.89 kgm^{-2}, respectively, which corresponded to the average relative errors of 29.2% and 20.2%. Endalew *et al.* [37] found that the maximum RMS error was 1.68m s^{-1} and relative error was 11.04% for simulated peak air velocities around a fully branch-modeled pear tree.

E. VERIFICATION OF THE AIRFLOW VELOCITY FORMULA IN THE CENTRAL PLANE

In order to further verify the airflow velocity formula in the central plane, the experimental data, the calculated results from Formula (5), and the simulated results were compared at a fan speed of 1500 r min^{-1}. Fig. 13 demonstrates that the overall trend indicates that the calculation, simulated, and test results all displayed a similar trend: the air velocity gradually decreased from the center line to the air flow boundary in the same section for the given distance from the air supply, and the farther the measurement points from the outlet, the lower the wind speed. From the point of view of the numerical error, there were some errors between the calculated, simulated, and experimental values; and the errors were mostly lower than 20%. Therefore, the central plane airflow velocity formula was able to accurately reflect the distribution of the air flow field in the central plane of the multi-channel air-assisted orchard sprayer.

IV. CONCLUSIONS

(1) For different fan speeds (600, 900, 1200, 1500, and 1800 r min^{-1}), the air flow field of the multi-channel air assisted sprayer was axisymmetric in the central plane, and the air velocity on the center line first increased and then attenuated exponentially. Within the range of the section 1.0 m from the outlet, a distinct air flow section was static due to the existence of low-pressure vortices between the adjacent outlets. Beyond this range, the four air streams mixed evenly, and the airflow velocity followed a Gaussian distribution at height y.

(2) The air flow field of the multi-channel air assisted sprayer exhibited an elliptical cross section at a distance from the outlet where $x > 1.0$ m. With the increase in the distance from the outlet, the distribution range of the velocity field became larger, and the multi-level elliptical distribution at the near end gradually developed into a small-level elliptical distribution at the far end of the model. The distribution of the elliptical airflow boundary could be obtained when the distance from the outlet was $x > 1.0$ m.

(3) Different distances from the air supply significantly influenced the fluctuation of the air flow. When the speed of the fan was 1500 r min^{-1}, the distance from the air supply should be in the range of 0.5–1.0 m, and the air flow coverage should be in the range of 0.7–2.1 m, which will meet the requirements of spindle fruit tree profiling. When the distance between the outlets was fixed, according to the dimensionless treatment of the velocity curves of each section, the speed of the fan did not significantly affect the position of the confluence point and the velocity fluctuation in each section.

REFERENCES

[1] S. A. Svensson, R. D. Brazee, R. D. Fox, and K. A. Williams, "Air jet velocities in and beyond apple trees from a two–fan cross–flow sprayer," *Trans. ASAE*, vol. 46, no. 3, pp. 611–621, Jun. 2003.
[2] B. Panneton, B. Lacasse, and M. Piché, "Effect of air-jet configuration on spray coverage in vineyard," *Biosyst. Eng.*, vol. 90, no. 2, pp. 173–184, Feb. 2005.
[3] A. M. Endalew, C. Debaer, N. Rutten, J. Vercammen, M. A. Delele, H. Ramon, and P. Verboven, "A new integrated CFD modelling approach towards air-assisted orchard spraying. Part I. Model development and effect of wind speed and direction on sprayer airflow," *Comput. Electron. Agricult.*, vol. 71, no. 2, pp. 128–136, May 2010.
[4] S.-W. Hong, L. Zhao, and H. Zhu, "CFD simulation of airflow inside tree canopies discharged from air-assisted sprayers," *Comput. Electron. Agricult.*, vol. 149, pp. 121–132, Jun. 2018.
[5] G. C. Randall, "The relationship of arterial blood pH and pCO_2 to the viability of the newborn piglet," *Can. J. Comparative Med.*, vol. 35, no. 2, pp. 141–146, 1971.
[6] J. V. Cross, P. J. Walklate, R. A. Murray, and G. M. Richardson, "Spray deposits and losses in different sized apple trees from an axial fan orchard sprayer: 3. Effects of air volumetric flow rate," *Crop Protection*, vol. 22, no. 2, pp. 381–394, 2003.
[7] M. A. Delele, A. De Moor, B. Sonck, H. Ramon, B. M. Nicolaï, and P. Verboven, "Modelling and validation of the air flow generated by a cross flow air sprayer as affected by travel speed and fan speed," *Biosyst. Eng.*, vol. 92, no. 2, pp. 165–174, May 2005.
[8] R. D. Fox, R. C. Derksen, H. Zhu, R. D. Brazee, and S. A. Svensson, "A history of air-blast sprayer development and future prospects," *Trans. ASABE*, vol. 51, no. 2, pp. 405–410, May/Apr. 2008.
[9] R. C. Derksen and R. L. Gray, "Deposition and air speed patterns of air-carrier apple orchard sprayers," *Trans. ASAE*, vol. 38, no. 1, pp. 5–11, Jan./Feb. 1995.
[10] L. R. Khot, R. Ehsani, G. Albrigo, A. J. Landers, and P. A. Larbi, "Spray pattern investigation of an axial-fan airblast precision sprayer using a modified vertical patternator," *Appl. Eng. Agricult.*, vol. 28, no. 5, pp. 5–11, Jan./Feb. 2012.
[11] A. T. Duga, D. Dekeyser, K. Ruysen, D. Bylemans, D. Nuyttens, B. M. Nicolaï, and P. Verboven, "Numerical analysis of the effects of wind and sprayer type on spray distribution in different orchard training systems," *Boundary-Layer Meteorol.*, vol. 157, no. 3, pp. 517–535, Dec. 2015.
[12] A. Godyn, R. Holownicki, G. Doruchowski, and W. Swiechowski, "Dual-fan orchard sprayer with reversed air-stream—Preliminary trials," *Agricult. Eng. Int. CIGR J.*, vol. X, May 2008.
[13] A. Godyn, R. Holownicki, G. Doruchowski, and W. Swiechowski, "Dual-fan orchard sprayer with reversed air-stream—Preliminary trials," presented at the 9th Workshop Sustain. Plant Protection Techn. Fruit Growing, Alnarp, Sweden, Sep. 2007.
[14] C. Wellington, J. Campoy, L. Khot, and R. Ehsani, "Orchard tree modeling for advanced sprayer control and automatic tree inventory," in *Proc. IEEE/RSJ Int. Conf. Intell. Robots Syst. (IROS) Workshop Agricult. Robot.*, Vilamoura, Portugal, Oct. 2012.
[15] A. T. Duga, A. M. Endalew, B. M. Nicolaï, P. Verboven, D. Dekeyser, D. Nuyttens, and N. Hendrickx, "Fluid dynamics modelling of orchard sprayer performance: Machine type and operational parameters characterization," in *Proc. 1st Int. Symp. CFD Appl. Agricult.*, Valencia, Spain, 2012, pp. 251–257.
[16] G. Doruchowski, W. Swiechowski, R. Holownicki, and A. Godyn, "Environmentally-dependent application system (EDAS) for safer spray application in fruit growing," in *Proc. 1st Int. Symp. CFD Appl. Agricult.*, Valencia, Spain, 2012, pp. 251–257.
[17] G. Doruchowski, W. Swiechowski, A. Godyn, and R. Holownicki, "Automatically controlled sprayer to implement spray drift reducing application strategies in orchards," *J. Fruit Ornamental Plant Res.*, vol. 19, no. 1, pp. 175–182, 2011.
[18] A. J. Landers, "Developments towards an automatic precision sprayer for fruit crop canopies," presented in the ASABE Annu. Int. Meeting, Pittsburgh, PA, USA, Jun. 2010.

[19] Q. Wei, Z. Sanqin, D. Weimin, S. Chengda, L. Jiang, L. Yinian, and G. Jiabing, "Effects of fan speed on spray deposition and drift for targeting air-assisted sprayer in pear orchard," *Int. J. Agricult. Biol. Eng.*, vol. 9, no. 4, pp. 53–62, Sep. 2016.
[20] R. Hołownicki, G. Doruchowski, W. Świechowski, A. Godyń, and P. J. Konopacki, "Variable air assistance system for orchard sprayers; concept, design and preliminary testing," *Biosyst. Eng.*, vol. 163, pp. 134–149, Nov. 2017.
[21] Y. Wu, X. Cheng, W. Ding, M. Xiao, J. Gu, and W. Qiu, "Structural optimization of the rear arc cover of a multi-channel air-assisted sprayer," *Int. Agricult. Eng. J.*, vol. 27, no. 2, pp. 73–81, 2018.
[22] O. Kira, Y. Dubowski, and R. Linker, "*In-situ* open path FTIR measurements of the vertical profile of spray drift from air-assisted sprayers," *Biosyst. Eng.*, vol. 169, pp. 21–32, May 2018.
[23] R. D. Fox, R. D. Brazee, S. A. Svensson, and D. L. Reichard, "Air-jet velocities from a cross-flow fan sprayer," *Trans. ASAE*, vol. 35, no. 5, pp. 1381–1382, 1992.
[24] M. Klein, A. Sadiki, and J. Janicka, "Investigation of the influence of the Reynolds number on a plane jet using direct numerical simulation," *Int. J. Heat Fluid Flow*, vol. 24, no. 6, pp. 785–794, Dec. 2003.
[25] F. J. García-Ramos, M. Vidal, A. Boné, H. Malón, and J. Aguirre, "Analysis of the air flow generated by an air-assisted sprayer equipped with two axial fans using a 3D sonic anemometer," *Sensors*, vol. 12, no. 6, pp. 7598–7613, Jun. 2012.
[26] J. A. R. Ramón, D. L. Sánchez, M. H. Zaldívar, and U. Pal, "Morphology and defect evolution in vapor-grown In2O3:Sn micro-/nanoparticles," *Mater. Sci. Semicond. Process.*, vol. 40, pp. 943–953, Dec. 2015.
[27] F. Wang, "Basic knowledge of computational fluid dynamic," in *Computational Fluid Dynamics Analysis-CFD Software Principles and Applications*. Beijing, China: Tsinghua Univ. Press, 2004.
[28] L. Zhou, X. Zhang, X. Lu, and S. Ding, "Wind performance numerical simulation and test of disk nebulizer," *Trans. Chin. Soc. Agricult. Mach.*, vol. 44, no. 10, pp. 72–75, 2012.
[29] J. Chen, S. Song, D. Su, S. Hong, and L. Zhang, "Test on airflow field and spray characteristics for long-range air-blast sprayer," *Trans. Chin. Soc. Agricult. Eng.*, vol. 33, no. 24, pp. 72–79, 2017.
[30] G. K. Batchelor, *An Introduction to Fluid Dynamics*. London, U.K.: Cambridge Univ. Press, 1967.
[31] A. Koestel and J. B. Austin, "Austin Air velocities in two parallel ventilating jets," *ASHAE Trans.*, no. 62, pp. 425–437, 1956.
[32] Y. Xiao, X. Liu, and Y. Yang, "Study on coincidence characteristics of air supply outlets in large space layout," *Ventilation Dust Removal*, no. 3, pp. 1–5, 1997.
[33] S. Song, T. Hong, H. Liu, Y. Ruan, and J. Chen, "Distribution of airflow velocity in wide spray air sprayer," *Trans. Chin. Soc. Agricult. Eng.*, vol. 29, no. 24, pp. 17–24, 2013.
[34] A. T. Duga, M. A. Delele, K. Ruysen, D. Dekeyser, D. Nuyttens, D. Bylemans, B. M. Nicolaï, and P. Verboven, "Development and validation of a 3D CFD model of drift and its application to air-assisted orchard sprayers," *Biosyst. Eng.*, vol. 154, pp. 62–75, Feb. 2017.
[35] J. Badules, M. Vidal, A. Boné, J. Llop, R. Salcedo, E. Gil, and F. J. García-Ramos, "Comparative study of CFD models of the air flow produced by an air-assisted sprayer adapted to the crop geometry," *Comput. Electron. Agricult.*, vol. 149, pp. 166–174, Jun. 2018.
[36] A. M. Endalew, C. Debaer, N. Rutten, J. Vercammen, M. A. Delele, H. Ramon, B. M. Nicolaï, and P. Verboven, "A new integrated CFD modelling approach towards air-assisted orchard spraying—Part II: Validation for different sprayer types," *Comput. Electron. Agricult.*, vol. 71, pp. 137–147, May 2010.

XIANGYUN CHAO was born in Changzhou, Jiangsu, China, in 1997. She received the B.S. degree in vehicle engineering from Nanjing Agricultural University, Nanjing, China, in 2019. She is currently pursuing the M.S. degree in power engineering with Zhejiang University, Zhenjiang, China.

From 2015 to 2019, she was a member of the Intelligent and Precision Pesticide Application and Agricultural Equipment Laboratory, Nanjing Agricultural University. Her research interests include profile modeling, multi-channel sprayer, and airflow distribution.

Ms. Chao's awards and honors include the National Scholarships, the Merit Students and The First Scholarship, and the Outstanding Graduate Award from Nanjing Agricultural University.

SHANG CHEN, photograph and biography not available at the time of publication.

WEI QIU received the B.S. degree in physics from Hubei Normal University, Hubei, China, in 2007, and the Ph.D. degree in agricultural mechanization engineering from Nanjing Agricultural University, Nanjing, China, in 2012.

Since 2012, he has been an Assistant Professor with the Agricultural Mechanization Engineering Department, Nanjing Agricultural University. He is the author of two books, more than 30 articles, and more than ten inventions. His research interests include intelligent and precision pesticide application.

Dr. Qiu was received the First Prize for Outstanding Teaching Achievements from Nanjing Agricultural University.

XIAOLAN LV, photograph and biography not available at the time of publication.

HUA LI, photograph and biography not available at the time of publication.

CHANGJIE HAN, photograph and biography not available at the time of publication.

FIAZ AHMAD, photograph and biography not available at the time of publication.